International Journal of Nanomedicine

Dovepress
Taylor & Francis Group

Open Access Full Text Article

ORIGINAL RESEARCH

ROS-Triggered Self-Aggregation of a β-Elemene Olefin-Rich Nanoemulsion for Mitochondrial-Targeted Metabolic Reprogramming and Colitis Inflammation Alleviation

Zhiyuan Luo[1–3,*], Luyu Jia[4,*], Yu Tang[2,*], Yifan Huang[5,*], Zhanni Ma[2,*], Youpeng Li[2], Xiaojing Zhang[2], Pengfei Zhang[2], Tian Xie[1,3]

[1]Innovation Research Institute of Traditional Chinese Medicine, Shanghai University of Traditional Chinese Medicine, Shanghai, 201203, People's Republic of China; [2]Institute of Molecular Immunology, School of Laboratory Medicine and Biotechnology, Southern Medical University, Guangzhou, Guangdong, 510000, People's Republic of China; [3]Key Laboratory of Elemene Class Anti-Cancer Chinese Medicines, Engineering Laboratory of Development and Application of Traditional Chinese Medicines, Collaborative Innovation Center of Traditional Chinese Medicines of Zhejiang Province, School of Pharmacy, Hangzhou Normal University, Hangzhou, Zhejiang, 310000, People's Republic of China; [4]The Second Clinical College of Guangzhou University of Chinese Medicine, Guangzhou, Guangdong, 510120, People's Republic of China; [5]School of Statistics, Beijing Normal University, Beijing, 100000, People's Republic of China

*These authors contributed equally to this work

Correspondence: Tian Xie, Innovation Research Institute of Traditional Chinese Medicine, Shanghai University of Traditional Chinese Medicine, Shanghai, 201203, People's Republic of China, Email tianxie@hznu.edu.cn; Pengfei Zhang, Institute of Molecular Immunology, School of Laboratory Medicine and Biotechnology, Southern Medical University, Guangzhou, Guangdong, 510000, People's Republic of China, Email zpf0418@i.smu.edu.cn

Purpose: Inflammatory bowel disease (IBD) is a chronic condition driven by pro-inflammatory macrophages. Although natural compounds with carbon–carbon double bonds (C=C bonds), such as β-elemene, exhibit anti-inflammatory properties, their precise subcellular targets and mechanisms remain elusive. This study aimed to develop a targeted nanomedicine to elucidate the anti-inflammatory mechanism of β-elemene and establish a novel therapeutic strategy for colitis.

Patients and Methods: We engineered a reactive oxygen species (ROS)-responsive β-elemene nanoemulsion (ELE-NE) for targeted drug delivery. Its therapeutic efficacy and mechanism were evaluated in a murine model of dextran sulfate sodium (DSS)-induced colitis. A mitochondria-targeted, ROS-activatable near-infrared probe was also developed for in vivo imaging tracking of inflammatory foci and assessment of therapeutic efficacy.

Results: In DSS-induced colitis mice, ELE-NE preferentially accumulated in inflamed colon tissue and effectively alleviated disease pathology. Mechanistically, upon reaching inflammatory macrophages, ELE-NE utilized the pathological ROS surge to undergo spatially confined aggregation at mitochondrial sites. This nano-aggregation directly disrupted the electron transport chain (ETC), potently suppressing oxidative phosphorylation and reprogramming cellular energy metabolism. Consequently, this mitochondria-focused metabolic intervention attenuated M1 macrophage polarization, reduced pro-inflammatory cytokine secretion.

Conclusion: This is the first report demonstrating that β-elemene acts via ROS-triggered mitochondrial aggregation and metabolic reprogramming. We deciphered the mechanism of β-elemene, revealing that its olefinic (C=C) functional group enables bioresponsive mitochondrial aggregation and metabolic reprogramming, thereby proposing the concept of "olefinic drugs" as a distinct therapeutic class. Furthermore, we established a novel theranostic paradigm for treating inflammatory diseases using olefinic nanomedicines, enabled by a companion imaging tool for non-invasive detection of inflammatory foci and dynamic monitoring of the treatment process.

Keywords: colitis, β-elemene, ROS-triggered, self-aggregation, energy metabolism

https://doi.org/10.2147/IJN.S599389
Received: 10 February 2026
Accepted: 6 May 2026
Published: 8 June 2026

Graphical Abstract

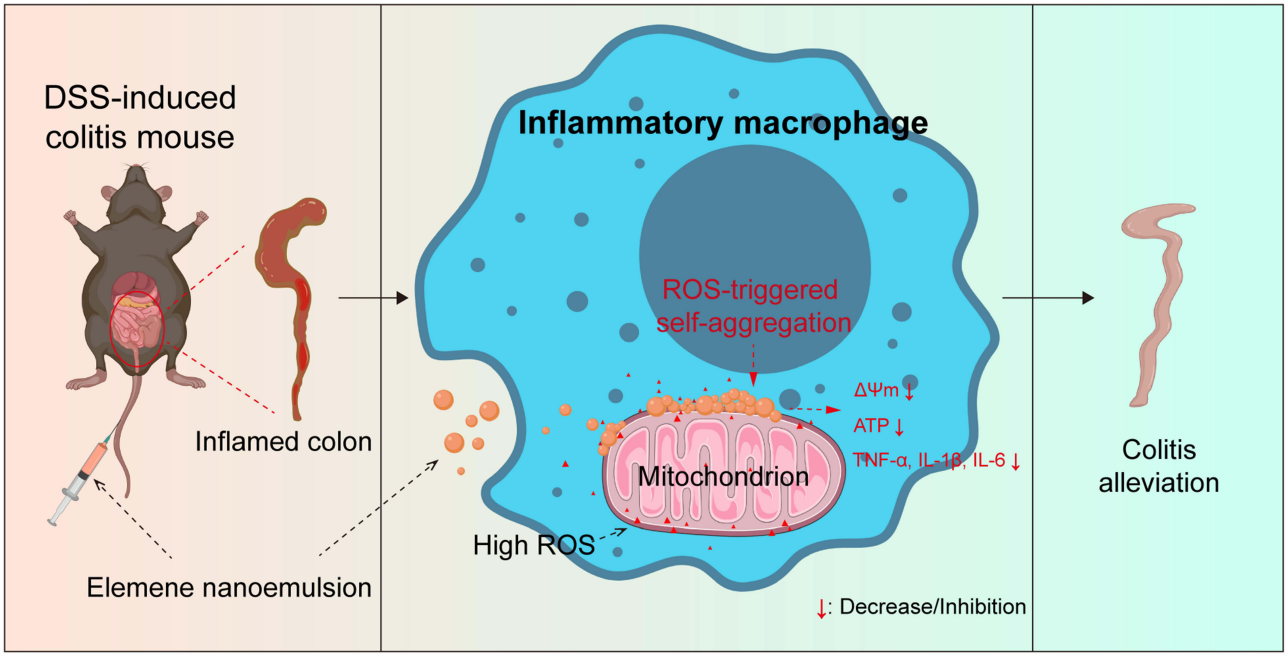

Introduction

Inflammatory bowel disease (IBD), including ulcerative colitis and Crohn's disease, is a group of chronic, immune-mediated disorders driven by intestinal inflammation.[1–4] A hallmark of IBD pathogenesis is the aberrant infiltration of immune cells into the gastrointestinal tract and the subsequent activation of complex inflammatory networks.[4–6] While intestinal homeostasis relies on a precise balance between pro- and anti-inflammatory signals, this equilibrium is profoundly disrupted in IBD.[6,7] A key driver of this pathology is the pervasive infiltration of M1 macrophages, which sustains disease progression through the rampant secretion of pro-inflammatory cytokines such as TNF-α, IL-1β, and IL-6.[8–10] Critically, the pro-inflammatory polarization of M1 macrophages is characterized by a metabolic shift toward aerobic glycolysis, accompanied by impairment of the tricarboxylic acid (TCA) cycle and mitochondrial oxidative phosphorylation (OXPHOS), positioning the mitochondrion as a potential therapeutic node.[11–14]

The therapeutic landscape for IBD, long dominated by aminosalicylates, corticosteroids, and immunomodulators, is expanding to include novel anti-inflammatory agents.[15–18] Despite these options, current treatments are often limited by insufficient efficacy, significant adverse effects, and the emergence of drug resistance, underscoring an urgent unmet need for safer and more targeted therapies.[19–21] Recent explorations have ranged from inorganic elements (eg., selenium, arsenic) and Mn_3O_4 nanozymes to natural compounds like ellagic acid and curcumin, which often act through NF-κB pathway inhibition.[9,22–25] Among natural products, terpenoids constitute the largest and most structurally diverse family of secondary metabolites, classified by their isoprene units.[26–28] A prominent member is the sesquiterpene β-elemene (ELE), isolated from Curcuma wenyujin, which has been extensively studied for its antitumor properties.[29–32] Beyond oncology, ELE exhibits a broad spectrum of bioactivities, including antioxidant, cardiovascular protective, and anti-inflammatory effects.[33–35] Notably, the olefinic (C=C) structure of β-elemene, while critical for its bioactivity, remains largely unexplored as a responsive motif for stimuli-triggered drug delivery in inflammatory microenvironments.

ELE exhibits broad anti-inflammatory efficacy across disease models. It alleviates hepatic fibrosis in rats by reducing plasma endotoxin, serum TNF-α, and hepatic CD14, and mitigates neuroinflammation by suppressing inflammatory mediators and neuronal apoptosis.[36–39] Despite these pharmacological observations, the initial molecular events and

direct subcellular targets of ELE remain elusive, which represents a fundamental gap in understanding the action mode of not only ELE but also numerous terpenoid natural products.

To enable targeted therapy for inflammatory bowel disease, we engineered a uniform β-elemene nanoemulsion (ELE-NE) using HS-15, effectively addressing the pharmaceutical limitations of the hydrophobic compound (Figure 1).[40] We strategically leveraged the pathological overproduction of reactive oxygen species (ROS)—a well-defined feature of the IBD microenvironment that drives mucosal redox imbalance—as a key targeting cue for drug delivery.[41–43] Crucially, we demonstrate that ELE's olefinic architecture confers an intrinsic capacity for ROS-triggered molecular aggregation. This triggered self- aggregation directly mediates the selective enrichment of ELE-NE on mitochondrial membranes of M1 macrophages, inducing a metabolic reprogramming that suppresses pro-inflammatory polarization and ameliorates experimental colitis. This mechanism establishes the carbon–carbon double bond as a fundamental structural determinant governing immunometabolic modulation, which we term "olefinic drugs." The known immunometabolic activities of various C=C-rich natural products support the plausibility and further development of this conceptual framework.[44–48] Leveraging this targeting paradigm, we designed a companion ROS-triggered near-infrared (NIR) probe that co-localizes with inflammatory foci. The probe facilitates non-invasive spatiotemporal tracking of disease progression through real-time in vivo imaging, providing a direct visual readout of therapeutic efficacy. This integrated design—pairing a therapeutic nanoemulsion with a companion diagnostic probe—follows the emerging paradigm of inflammation-targeted theranostics, which seeks to unify disease localization and therapeutic intervention within a single nanomedicine platform.[49,50]

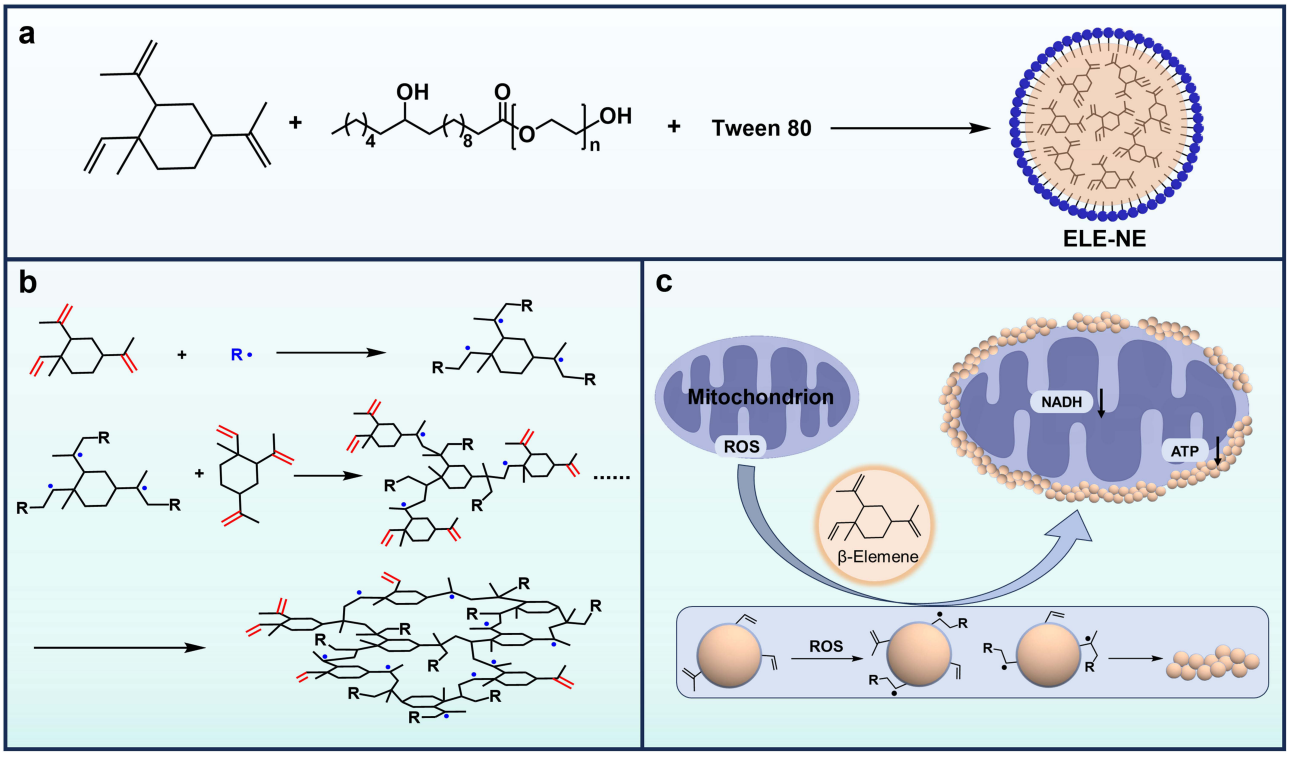

Figure 1 Mechanism of the ROS-triggered olefinic nanoemulsion (β-elemene) in modulating macrophage inflammation via targeting mitochondrial energy metabolism. (**a**) Preparation of the ELE-NE. The ELE-NE was formulated by rapid homogenization of an ethanolic solution containing β-elemene and HS-15 in saline, using Tween 80 as a dispersant. (**b**) ROS-triggered self- aggregation mechanism. In the ROS-enriched inflammatory microenvironment, the electron-rich olefinic bonds of β-elemene undergo ROS-specific reactions, triggering in situ self- aggregation and the formation of nano-sized aggregates within the mitochondrial region. (**c**) Mitochondrial targeting and metabolic reprogramming by ELE-NE. ELE-NE preferentially targets mitochondria in inflammatory macrophages via its ROS-triggered property. The aggregates disrupt the electron transport chain, leading to mitochondrial membrane potential (ΔΨm) dissipation, suppression of ATP synthesis, and disruption of redox homeostasis. This metabolic reprogramming effectively suppresses the pro-inflammatory phenotype of M1 macrophages. In this figure, downward arrows (↓) denote decrease or inhibition.

https://doi.org/10.2147/IJN.S599389

Material and Methods

Reagents

All chemical reagents and assay kits were obtained from commercial suppliers and used according to the manufacturers' instructions. Kolliphor® HS-15 (Solutol® HS-15, Macrogol 15 Hydroxystearate) was obtained from Sigma-Aldrich (USA). β-Elemene (purity ≥98%), polysorbate 80 (Tween-80), and dextran sulfate sodium (DSS) were sourced from Aladdin (China). Enzyme-linked immunosorbent assay (ELISA) kits were acquired from Meimian (China). The following commercial assay kits were utilized for key functional analyses: Cell Counting Kit-8 (CCK-8; APExBIO, USA), GSH/GSSG-Glo™ Assay Kit (Promega, USA), Extracellular Oxygen Consumption Assay Kit (Abcam, UK), and JC-1 Mitochondrial Membrane Potential Assay Kit (Beyotime Biotechnology, China). Red blood cell lysis buffer was obtained from Solarbio (China). Fluorescent dyes 1,1'-dioctadecyl-3,3,3',3'-tetramethylindotricarbocyanine iodide (DiR) and 3,3'-dioctadecyloxacarbocyanine perchlorate (DiO) were purchased from MedChemExpress (USA) and Beyotime Biotechnology (China), respectively. The following reagents and antibodies from BioLegend (USA) were used: Zombie Aqua™ Fixable Viability Kit (423101), and TruStain FcX™ anti-mouse CD16/32 (Clone 93, Cat#101319). Fluorochrome-conjugated antibodies included: APC anti-mouse CD3 (Clone 17A2, Cat#100236), FITC anti-mouse CD3 (Clone 17A2, Cat#100203), FITC anti-mouse F4/80 (Clone BM8, Cat#123108), APC anti-mouse CD11c (Clone N418, Cat#117310).

Isolation, Differentiation, and Polarization of Bone Marrow-Derived Macrophages

Bone Marrow Harvest and Primary Cell Isolation

Bone marrow was aseptically flushed from femurs and tibiae of 6–8-week-old male C57BL/6 mice using ice-cold RPMI-1640 medium. The cell suspension was filtered through a 70-μm strainer and centrifuged (500 ×g, 5 min, 4 °C). Erythrocytes were lysed with 1× red blood cell lysis buffer for 5 min at room temperature. After washing with PBS, viable cells were counted and resuspended in complete growth medium: RPMI-1640 supplemented with 10% heat-inactivated fetal bovine serum (FBS), 100 U/mL penicillin, and 100 U/mL streptomycin.

Differentiation into M0 Macrophages

Cells were seeded at a density of 1×10^6 cells per 10-cm dish and incubated overnight (approximately 16 h) at 37 °C under 5% CO_2 to allow stromal cell attachment. Non-adherent hematopoietic progenitor cells were then transferred to new dishes and cultured for 7 days in complete medium containing 20 ng mL^{-1} recombinant murine macrophage colony-stimulating factor (M-CSF). The medium was replaced with fresh M-CSF-containing medium on day 3. By day 6, adherent cells had differentiated into quiescent M0 macrophages, which were detached using trypsin-EDTA for subsequent experiments.

Polarization to M1 Phenotype

M0 macrophages were polarized to the classical M1 phenotype by stimulation with 100 ng mL^{-1} ultrapure lipopolysaccharide (LPS) for 48 h.

Synthesis of the ELE-NE

The β-elemene nanoemulsion was prepared via a facile emulsion/solvent diffusion method. Briefly, β-elemene (10 mg/mL) and HS-15 (40 mg/mL) were separately dissolved in absolute ethanol. Subsequently, 100 μL of the β-elemene solution was mixed with 50 μL of the HS-15 solution (mass ratio of 1:2). The resulting ethanolic mixture was injected dropwise (at a rate of ~1 mL/min) into 2 mL of saline under continuous magnetic stirring (400 rpm). After stirring for 1 h at room temperature, Tween-80 was added as a stabilizer to a final concentration of 0.5 mg/mL, and stirring continued for an additional 25 min. The final formulation, designated ELE-NE, contained β-elemene at a concentration of 0.5 mg/mL and was stored at 4 °C for further use.[51]

Characterizations of ELE-NE

For physicochemical characterization, ELE-NE was formulated in deionized water to prevent interference from inorganic salts present in saline. To study free radical-induced aggregation, ELE-NE (2 mL, 0.5 mg/mL in H_2O) was treated with ammonium

persulfate (APS) and tetramethylethylenediamine (TEMED) (100 μM each) to generate free radicals. The mixture was stirred at room temperature for 24 h, and the resulting ELE-NE aggregates were harvested for subsequent analysis.

The morphology of pristine and free radical-aggregated ELE-NE was characterized by transmission electron microscopy (TEM; FEI Tecnai20) at a 200 kV acceleration voltage. For TEM imaging, a sample droplet was applied to a 200-mesh carbon-coated copper grid, blotted to remove excess liquid, and air-dried. Hydrodynamic diameter was assessed by dynamic light scattering (DLS) using a Malvern Zetasizer Nano ZS system.

Gel permeation chromatography (GPC) was employed to analyze the reaction products. An ethanolic β-elemene solution (100 μL, 10 mg/mL) was mixed with an aqueous solution of APS and TEMED (1 mL, 100 μM each). The reaction proceeded for 24 h at room temperature with stirring (400 rpm), after which the solvent was removed. The residue was dissolved in dimethyl sulfoxide (DMSO), which also functioned as the mobile phase. Molecular weight distribution was determined using an Agilent 1260 Infinity II GPC system, with untreated β-elemene as the control. Data were processed and visualized with GraphPad Prism 10.

Cell Viability Assay

Cytotoxicity was evaluated using the Cell Counting Kit-8 (CCK-8; APExBIO, USA). BMDMs were first polarized into the M1 phenotype by treatment with 100 ng/mL LPS for 48 h. The cells were then collected and seeded into 96-well plates at a density of 6,000 cells per well. Following overnight adhesion, the cells were exposed to serially diluted ELE-NE (10–200 μg/mL) for 32 h. After treatment, 10 μL of CCK-8 reagent was added to each well, and the plates were incubated at 37 °C for 1 h. Absorbance was measured at 450 nm using a BioTek Epoch microplate reader. Cell viability was expressed as a percentage relative to untreated control cells after blank subtraction. Data represent the mean ± standard deviation (s.d.) of five technical replicates per condition from three independent biological experiments. Statistical analysis was performed using one-way ANOVA in GraphPad Prism 10.

ELISAs

To assess the effect of ELE-NE on the inflammatory response, M1-polarized macrophages were treated with increasing concentrations of ELE-NE (40, 60, and 70 μg/mL) for 48 hours (n = 5). Culture supernatants were then collected, and the secretion levels of IL-1β, IL-6, and TNF-α were quantified using commercial ELISA kits (MEIMIAN) according to the manufacturer's instructions. Absorbance was measured at 450 nm using an Epoch microplate spectrophotometer, and data from three independently experiments were analyzed with GraphPad Prism 10 software.

Confocal Microscopy Analysis

Bone marrow-derived macrophages (BMDMs) were plated on glass coverslips and assigned to different treatment groups to establish distinct cellular models: M0 (untreated), M1 (polarized with 100 ng/mL LPS for 48 h), and mitochondrial stress (treated with 2 μM Antimycin A for 8 h). All groups were then incubated for 48 h with 40 μg/mL of ELE-NE, free β-elemene (Free ELE) or blank nanoemulsion (Blank-NE), which had been pre-labeled with 1 μM DiO (Beyotime). Following treatment, cells were washed with PBS and stained with MitoTracker™ Red FM (Invitrogen) for mitochondria and Hoechst 33342 (Beyotime) for nuclei. Coverslips were mounted in fresh pre-warmed medium, and images were acquired using a laser scanning confocal microscope (LSM 880). Images were visualized using ZEISS ZEN 3.10 software. Colocalization of DiO-labeled ELE-NE (green) with MitoTracker Red (red) was quantified using ImageJ/Fiji software, with the Pearson's correlation coefficient calculated. All quantitative data were obtained from three independent experiments.

Mitochondrial Membrane Potential

Mitochondrial membrane potential (ΔΨm) was assessed using the JC-1 Assay Kit (Beyotime). LPS-induced M1 macrophages were seeded on coverslips in 6-well plates and treated with 40 μg/mL ELE-NE or PBS for 48 h. Cells were then washed with pre-warmed PBS and incubated with 1 mL of JC-1 working solution at 37 °C for 20 min in the dark. The working solution was prepared by diluting the 200× JC-1 stock in 1× staining buffer per the manufacturer's protocol. After incubation, cells were washed twice with JC-1 staining buffer to remove unbound dye. Nuclei were

counterstained with DAPI (Beyotime), and images were acquired on an LSM 880 confocal microscope. Images were visualized using ZEISS ZEN 3.10 software. Evaluation of membrane potential changes through fluorescence alterations in JC-1 aggregates (red) and monomers (green).

Oxygen Consumption Measurements

Macrophage mitochondrial respiration was quantified using the Extracellular Oxygen Consumption Assay Kit (Abcam). Bone marrow-derived M0 macrophages were polarized with LPS (100 ng/mL) to the M1 phenotype, seeded in 96-well plates (1×10^4 cells/well), and treated for 24 h with ELE-NE (40, 60, or 70 μg/mL) or PBS (n = 5). Following the addition of 10 μL O_2-sensitive probe to each well, reactions were immediately overlaid with 100 μL high-sensitivity mineral oil to create a sealed microenvironment. Fluorescence (Ex/Em 380/650 nm) was measured at 1.5-min intervals for 120 min. Data from three independently experiments were analyzed in GraphPad Prism 10.

Measurement of Intracellular GSH and GSSG Levels

The intracellular glutathione redox state was determined using the GSH/GSSG-Glo™ Assay Kit. Bone marrow-derived M0 macrophages were polarized to the M1 phenotype with LPS (100 ng/mL) and seeded in 96-well plates at 1×10^4 cells/well. Cells were then treated for 24 h with ELE-NE (40, 60, or 70 μg/mL) or PBS (n=5). After treatment, the medium was aspirated, and cells were lysed in 50 μL of the designated lysis reagent for parallel measurement of total and oxidized glutathione, using cell-free wells as blanks. Following 5 min of shaking, 50 μL of Luciferin Generation Reagent was added, and the plate was incubated for 30 min. Luminescence was recorded after the addition of 100 μL Luciferin Detection Reagent and a 15-min stabilization period. The GSH/GSSG ratio was calculated as (Total Glutathione – 2 × GSSG) / GSSG. For all measurements, background luminescence from cell-free blank wells was subtracted prior to calculation. Absolute glutathione concentrations were derived from a standard curve generated with reference samples provided in the kit according to the manufacturer's instructions. Values were then normalized to the initial number of cells seeded per well (parallel wells were seeded at identical density). Data from three independent experiments were analyzed using GraphPad Prism 10.

Cellular ATP Measurement

Intracellular ATP levels were quantified using a commercial assay kit (Beyotime) and normalized to total protein concentration. M1-polarized macrophages were plated in 6-well plates at 5×10^5 cells/well and allowed to adhere overnight. Cells were treated for 24 h with ELE-NE (40, 60, or 70 μg/mL) or PBS vehicle (n=5). After treatment, cells were lysed in 200 μL of ice-cold lysis buffer, and the lysates were centrifuged at 12,000 ×g for 5 min at 4 °C. The resulting supernatant was collected for analysis. For the ATP assay, 100 μL of freshly prepared ATP detection reagent was dispensed into an opaque white luminometer plate and equilibrated for 5 min at room temperature. Then, 20 μL of each supernatant was injected, and luminescence was immediately measured using a GloMax® Discover Microplate Luminometer. Total protein concentration was determined in parallel by BCA assay for normalization. Data from three independent experiments were analyzed using GraphPad Prism 10.

Synthesis of the ROS-Triggered Near-Infrared Probe

To enable non-invasive near-infrared imaging of inflammatory foci, we prepared a DiR-labeled β-elemene nanoemulsion (DiR-ELE-NE) serving as a ROS-triggered NIR imaging probe. Briefly, 100 μL of β-elemene ethanolic solution (10 mg/mL) was mixed with 50 μL of HS-15 ethanolic solution (40 mg/mL) and DiR working solution (final concentration 1 μM) to form the organic phase. Under continuous magnetic stirring at 400 rpm, the organic phase was slowly injected dropwise into 2 mL of physiological saline. After stirring for 1 h at room temperature, Tween-80 was added as a stabilizer (final concentration 0.5 mg/mL), and stirring was continued for an additional 25 min to yield the final DiR-labeled ELE-NE probe. The probe was stored at 4 °C protected from light until further use.

Vivo Near-Infrared Fluorescence Imaging

The in vivo targeting and imaging capability of the probe was evaluated in a dextran sulfate sodium (DSS)-induced colitis mouse model. Colitis was induced in C57BL/6 mice by administering 2% (w/v) DSS in drinking water for 8 consecutive days. DSS-treated and healthy control mice received an intravenous injection of DiR-ELE-NE probe (5 mg/kg) via the tail vein. Twenty-four hours post-injection, in vivo NIR fluorescence imaging of the abdominal region was performed using an In Vivo FX Pro Bruker imaging system. Acquired images were visualized using Bruker MI software (version 7.2.1).

Flow Cytometric Analysis

To identify the immune cell subsets targeted by DiR-ELE-NE within the inflamed intestine, single-cell suspensions were prepared from intestinal tissues of DSS-induced colitis mice and healthy controls following intravenous administration of DiR-ELE-NE (5 mg/kg) as described in the preceding subsection. Briefly, mice were euthanized 24 h post-injection, and intestines were harvested, flushed with PBS, and minced into ~1 mm^3 fragments. Tissue digestion was performed for 60 min at 37 °C with gentle shaking in RPMI-1640 complete medium containing 2 mg/mL collagenase IV (MCE), 2.5 mg/mL Liberase (Roche), and 0.1 mg/mL DNase I (Sigma-Aldrich). The resulting cell suspension was filtered through a 70-μm cell strainer, and fibroblasts were removed by differential adhesion.

For flow cytometric staining, cells were first incubated with an anti-CD16/32 antibody (BioLegend) to block Fc receptors. Surface staining was then performed using fluorochrome-conjugated antibodies against CD3, F4/80, and CD11c (BioLegend), and 7-AAD was used to exclude dead cells. The frequency of DiR^+ cells was determined within each gated immune population. All data are representative of three independent experiments.

Animals

Female C57BL/6 mice (6–8 weeks old) from the Guangdong Experimental Animal Center were housed under standard conditions (12 h light/dark cycle, 25 °C) with ad libitum access to food and water. After acclimatization, mice were randomized into three groups (n = 5): healthy controls, DSS-colitis mice receiving PBS, and DSS-colitis mice treated with ELE-NE (5 mg/kg). Colitis was induced with 2% (w/v) DSS in drinking water for 8 days.[52] ELE-NE or PBS vehicle was administered intravenously on days 2, 4, 6, and 8. Body weight was tracked every other day until euthanasia and sample collection on day 9. All animal procedures were approved by the Animal Ethics Committee of Southern Medical University and performed in compliance with institutional ethical guidelines.

Biosafety Evaluation

To assess the systemic biosafety of ELE-NE, female C57BL/6 mice were randomized to receive intravenous injections of either ELE-NE (5 mg/kg) or PBS as a control (n = 3 mice per group). Dosing was performed every other day for a total of four administrations. On day 9, mice were euthanized, and blood was collected for serum separation. Comprehensive serum biochemical analysis was conducted to quantify markers of hepatic and renal function.

Statistical Analysis

Data are presented as the mean ± s.d. All statistical analyses were performed using GraphPad Prism 10. Specific tests were applied as follows: unpaired two-tailed Student's t-tests for comparisons between two groups; one-way ANOVA with Tukey's post hoc test for multiple comparisons; and two-way ANOVA with Tukey's post hoc test for datasets with two independent variables. A P value of less than 0.05 was considered statistically significant. Significance levels in figures are denoted as follows: *P < 0.05, **P < 0.01, ***P < 0.001, ****P < 0.0001; ns, not significant.

Results

Characterization and Radical-Triggered Response of β-Elemene Nanoemulsion

As a typical sesquiterpene hydrocarbon, ELE contains no polar functional groups, rendering it intrinsically hydrophobic and moderately volatile. These properties severely limit its aqueous solubility, thereby compromising bioavailability and

hindering efficient targeted delivery. To overcome these limitations, we developed a nanoemulsion-based delivery system (β-elemene nanoemulsion, ELE-NE) using the biocompatible surfactant HS-15 as the primary lipid carrier. ELE-NE was prepared by homogenizing ELE and HS-15 at a 1:2 mass ratio in ethanol, followed by slow injection into saline under continuous stirring. Tween-80 was incorporated as a dispersant (final concentration: 0.5 mg/mL) to form a uniform nanoemulsion with a final ELE concentration of 0.5 mg/mL.

TEM revealed well-dispersed and monodisperse nanoparticles with no detectable aggregation (Figure 2a), consistent with the morphology of an ideal nanocarrier capable of minimizing aggregation during systemic circulation. DLS further indicated a narrow size distribution, with the majority of particles ranging between 20 and 40 nm (Figure 2c, blue). Together, these data confirm the successful fabrication of a stable and uniform nano-delivery platform suitable for further biological evaluation.

To evaluate the cytotoxicity of ELE-NE, we treated mouse BMDMs—central effector cells in colitis—with increasing concentrations of the ELE nanoemulsion (10–200 μg/mL) for 48 h and assessed cell viability using a CCK-8 assay (Figure 2e). The nanoemulsion exhibited negligible cytotoxicity at concentrations up to 70 μg/mL, with cell viability remaining at approximately 99%. However, a slight yet significant reduction to 80.5 ± 2.8% was observed at 90 μg/mL. Further increasing the concentration resulted in a marked, dose-dependent decrease in viability, which plummeted to nearly complete cell death (3.50 ± 0.35%) at the highest concentration tested (200 μg/mL). This concentration-response profile establishes a therapeutic window for ELE-NE, with significant cytotoxicity occurring only beyond 70 μg/mL.

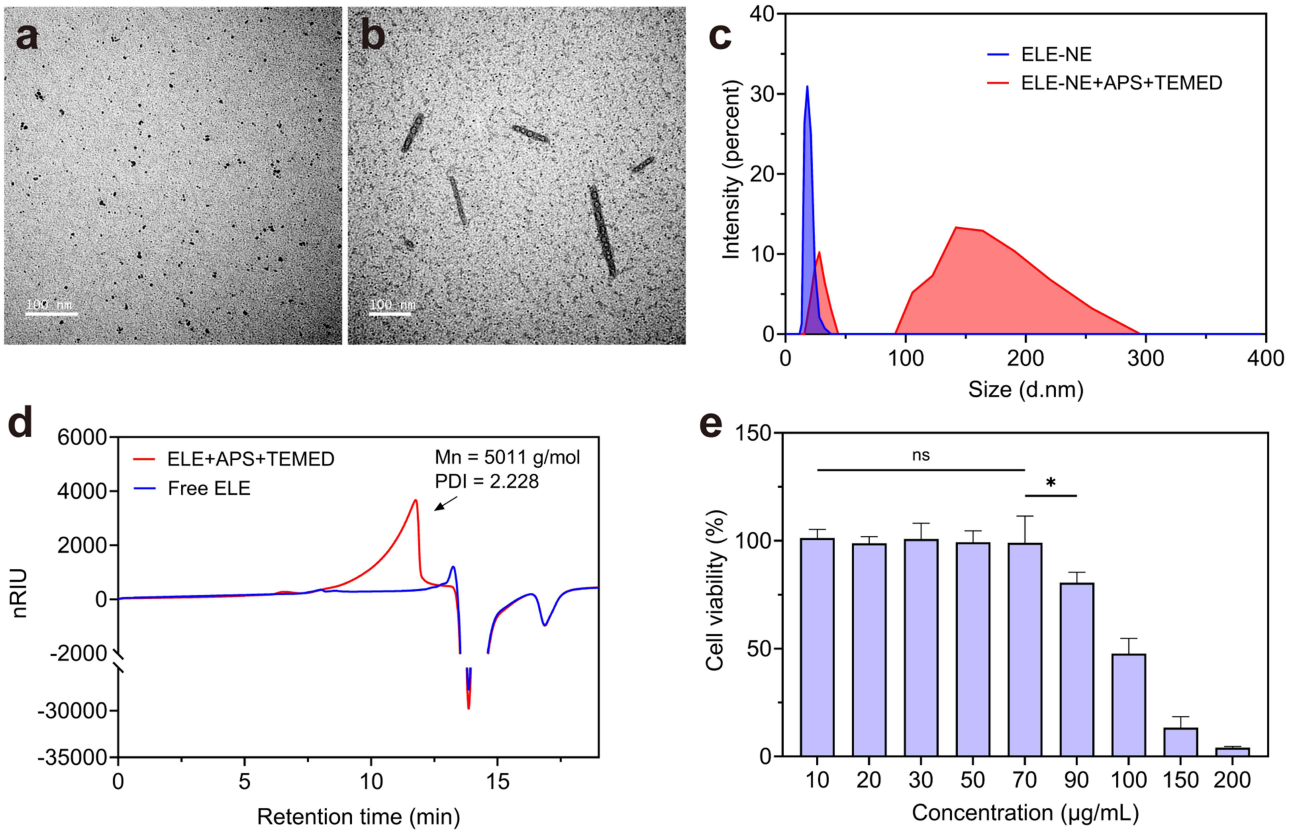

Figure 2 Physicochemical characterization, free radical-induced polymerization, and in vitro cytotoxicity of ELE-NE. (**a**) Representative TEM image of the freshly prepared ELE-NE. (**b**) Representative TEM image of the polymeric products formed after ELE-NE was treated with a free radical-initiation system containing APS and TEMED. Scale bars for (**a**) and (**b**): 100 nm. (**c**) Hydrodynamic size distribution profiles of pristine ELE-NE (blue) and free radical-induced polymeric products (red), as measured by DLS. (**d**) Molecular weight analysis by GPC comparing untreated free ELE and the products from free radical-induced polymerization of ELE. (**e**) Viability of BMDMs after 32 h treatment with a concentration gradient of ELE-NE, assessed by CCK-8 assay. Cells were seeded at 6,000 cells per well in a 96-well plate (n = 5). Data are representative of three independent experiments. Data in panel e are presented as mean ± s.d. and were analyzed by one-way ANOVA with Tukey's post hoc test. Significance levels are indicated as *p < 0.05 and ns (not significant).

https://doi.org/10.2147/IJN.S599389

To definitively investigate whether free radicals trigger the polymerization of ELE, we introduced APS and TEMED into ELE-NE to establish a controlled radical-generating system.[53–55] The mixture was incubated at room temperature for 24 hours, after which the resulting nanostructures were analyzed by TEM. TEM revealed a striking morphological shift: the initially spherical ELE-NE particles reorganized into needle-like structures over 100 nm in length (Figure 2b). This radical-induced self- aggregation is facilitated by the emulsion droplets, which concentrate both radicals and ELE molecules at the oil-water interface, thereby enhancing collision frequency and providing a localized environment conducive to polymerization.

DLS confirmed the polymerization, revealing a marked shift in the hydrodynamic diameter of ELE-NE from 20–40 nm to 100–300 nm upon radical treatment (Figure 2c, red). This size progression, consistent with the needle-like polymers observed by TEM, indicates the formation of well-defined aggregates. For molecular-scale validation, GPC of the radical-treated sample (in DMSO) displayed a distinct peak corresponding to a polymer with a number-average molecular weight (Mn) of 5011 g/mol (Figure 2d). No such peak was detected in the untreated ELE control, providing unambiguous evidence for radical-initiated polymerization of the olefin-rich compound. These results provide evidence for radical-initiated polymerization of the olefin-rich compound. Collectively, our findings establish a mechanistic foundation for ELE-NE's responsive activation within the ROS-enriched microenvironment characteristic of colitis.

ELE-NE Exhibits ROS-Dependent Mitochondrial Targeting and Suppresses Pro-Inflammatory Cytokine Production in Macrophages

To investigate the ROS dependence of ELE-NE's mitochondrial targeting in macrophages, we established in vitro models with varying levels of mitochondrial ROS (mtROS). Specifically, LPS was employed to induce M1 polarization along with mtROS generation,[56,57] and antimycin A, an electron transport chain inhibitor, was used to elicit a robust mtROS burst.[58–61] Free β-elemene (Free ELE) and blank nanoemulsion without β-elemene (Blank-NE) were included as controls. Following a 48-hour incubation of these models with DiO-labeled ELE-NE (40 μg/mL), mitochondria and nuclei were stained with MitoTracker Red CMXRos and Hoechst 33342, respectively, for confocal microscopy analysis, and colocalization was quantified using Pearson's correlation coefficient (PCC) (Figure 3a). In M0 macrophages, the green fluorescence of ELE-NE showed minimal overlap with the red mitochondrial signal. LPS-stimulated macrophages, however, exhibited partial colocalization. Most notably, antimycin A-treated macrophages—which sustained a potent mtROS burst—displayed the most intense colocalization (yellow), with PCC values significantly greater than those in the LPS group. In contrast, free ELE showed minimal cellular uptake and negligible mitochondrial colocalization across all conditions, while Blank-NE exhibited PCC values comparable to those of untreated controls. Together, the gradient of colocalization efficiency across M0, LPS-stimulated, and antimycin A-treated groups—observed exclusively for ELE-NE—provides compelling evidence that ELE-NE's mitochondrial targeting is directly proportional to and governed by the intracellular mtROS level, while also ruling out non-specific binding of the nanocarrier itself.

We next interrogated the functional consequences of ELE-NE's mitochondrial localization. Using the ΔΨm-sensitive dye JC-1,[62–64] we observed that ELE-NE treatment led to a marked decrease in mitochondrial membrane potential, as evidenced by a shift from red to green fluorescence (Figure 3b). This reduction in ΔΨm, consequent to mtROS-triggered ELE-NE accumulation, is consistent with compromised mitochondrial energy production, thereby proposing a plausible mechanism for its functional modulation of inflammatory macrophages.

To characterize the immunomodulatory capacity of ELE-NE, we measured its impact on pro-inflammatory cytokine secretion in LPS-induced M1 macrophages via ELISA. Treatment with increasing concentrations of ELE-NE (40, 60, and 70 μg/mL) resulted in a potent, dose-dependent suppression of all cytokines analyzed. TNF-α levels were markedly reduced (Figure 3c), reaching 306.3 ± 141.6 pg/mL at 70 μg/mL—approximately 16% of those in LPS-only controls. Secretion of IL-1β and IL-6 was similarly attenuated (Figure 3d and e), dropping to 18.3% and 19.7% of control levels, respectively, at the highest ELE-NE concentration (70 μg/mL). In contrast, free ELE was less effective at suppressing cytokine secretion at equivalent concentrations. Specifically, at 70 μg/mL, TNF-α levels remained around 53% of those in LPS-induced controls, with virtually no decrease at 40 μg/mL (Figure S1a). Likewise, at 70 μg/mL, IL-1β and IL-6 levels were only reduced to approximately 50% and 49% of control levels, respectively (Figure S1b and c). These data

 https://doi.org/10.2147/IJN.S599389

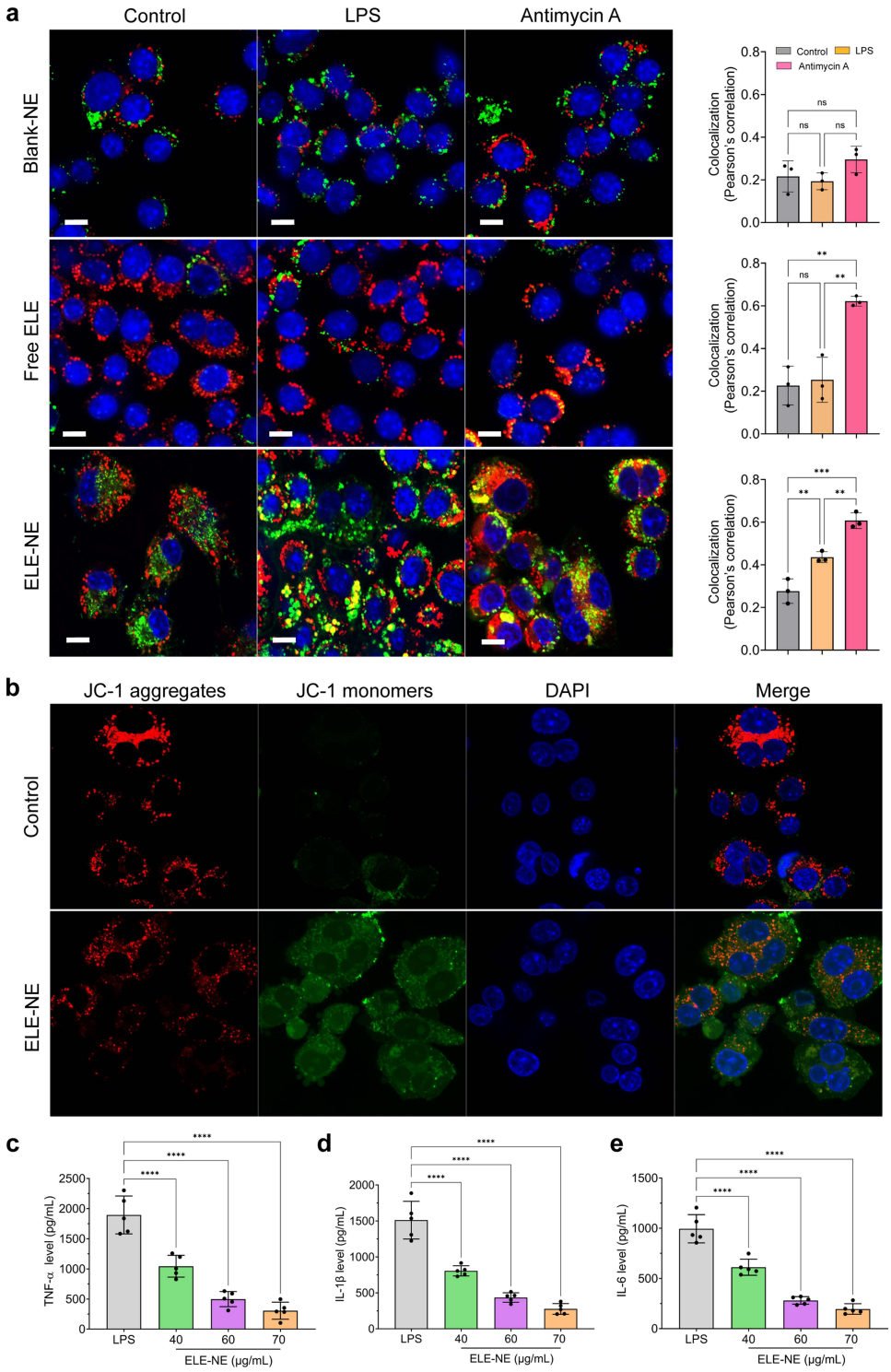

Figure 3 ELE-NE exhibits mtROS-triggered mitochondrial targeting and anti-inflammatory effects in macrophages. (**a**) Representative confocal microscopy images of DiO-labeled formulations (green) in bone marrow-derived macrophages (left), and quantification of colocalization between DiO and MitoTracker Red, expressed as Pearson's correlation coefficient (PCC) (right). Cells (M0, LPS-induced M1, or antimycin A-treated) were incubated with free β-elemene (Free ELE, 40 μg/mL), blank nanoemulsion without β-elemene (Blank-NE), or ELE-NE for 48 h. DiO was incorporated into all formulations for visualization. Subsequently, cells were stained with MitoTracker Red CMXRos (mitochondria, red) and Hoechst 33342 (nuclei, blue). Scale bar, 10 μm. (**b**) ΔΨm assessed by JC-1 fluorescence in LPS-induced M1 macrophages treated with PBS or ELE-NE (40 μg/mL) for 48 h. A shift from red (polarized) to green (depolarized) fluorescence indicates loss of ΔΨm. (**c–e**) ELISA quantification of pro-inflammatory cytokines TNF-α (**c**), IL-1β (**d**), and IL-6 (**e**) in supernatants from M1 macrophages treated with ELE-NE (40, 60, 70 μg/mL) for 48 h (n=5). Data are representative of three biologically independent experiments. Data are presented as mean ± s.d. and were analyzed by one-way ANOVA with Tukey's post hoc test. Significance levels are indicated as **p < 0.01, ***p < 0.001, ****p < 0.0001, and ns (not significant).

https://doi.org/10.2147/IJN.S599389

demonstrate that ELE-NE effectively blunts the inflammatory response in macrophages. This anti-inflammatory effect can be attributed to its mechanism of ROS-triggered mitochondrial targeting and the subsequent disruption of mitochondrial membrane potential.

ELE-NE Suppresses Mitochondrial Respiration and Electron Transfer

To determine the metabolic consequences of ELE-NE's mitochondrial targeting, we measured the oxygen consumption rate (OCR) as a proxy for oxidative phosphorylation.[63,65] In LPS-induced M1 macrophages, ELE-NE treatment for 48 h induced a concentration-dependent suppression of mitochondrial respiration (Figure 4a), reducing the OCR to 15.9% of control values at 70 μg/mL. In contrast, free ELE at an equivalent high concentration (70 μg/mL) only mildly decreased the OCR to 77.4% of the control level, indicating that efficient mitochondrial respiratory suppression requires nanoemulsion-mediated delivery. This progressive impairment is consistent with a disruption of electron transport chain (ETC) function.

We next assessed the impact on redox and energy metabolism. ELE-NE concentration-dependently depleted the GSH/GSSG ratio in M1 macrophages (Figure 4b), indicating oxidative stress compatible with ETC disruption. Free ELE (70 μg/mL) showed no significant effect on the GSH/GSSG ratio relative to untreated controls. Concurrently, intracellular ATP levels were severely compromised, dropping by approximately 75% at 70 μg/mL ELE-NE (0.54 ± 0.03 μmol/L) compared to untreated controls (2.17 ± 0.06 μmol/L) (Figure 4c). In comparison, free ELE (1.74 ± 0.14 μmol/L) at 70 μg/mL only decreased ATP levels by approximately 20% relative to untreated controls, a far weaker effect than that of ELE-NE. This concordant redox imbalance and energy failure demonstrate that ELE-NE disrupts mitochondrial OXPHOS, thereby precipitating a metabolic crisis in inflammatory macrophages. The markedly attenuated effects of free ELE further confirm that nanoemulsion encapsulation is essential for the full metabolic disruption exerted by β-elemene. We thus define a mechanism in which mitochondrial targeting of ELE-NE via ROS leads to ETC inhibition. The consequent collapse of respiration and redox balance impairs oxidative phosphorylation, culminating in a critical ATP deficit that metabolically undermines the pro-inflammatory activation of macrophages.

ELE-NE Targets Intestinal Inflammation in Mice

To assess the inflammatory site targeting of ELE-NE in vivo, we used the DSS-induced colitis model in C57BL/6J mice. Following intravenous administration of DiR-labeled ELE-NE to both DSS-treated and healthy control mice, near-infrared fluorescence imaging at 24 hours revealed a significantly stronger signal in the abdomens of colitis mice compared to controls (Figure 4d), indicating preferential accumulation at sites of inflammation. Ex vivo imaging of isolated colons confirmed this specific targeting to the inflamed intestinal tissue (Figure 4e). Quantitative analysis verified a dramatically higher fluorescence intensity in colitic mice, reaching 9.38-fold that of the healthy controls (Figure 4f).

To identify which immune cells in inflamed intestines are targeted by ELE-NE, we performed flow cytometry on single-cell suspensions from colonic tissues. In colitis mice, macrophages exhibited the highest DiR signal, with approximately 29% of cells being DiR^+ (Figure 4g)—representing an increase of approximately 3.4-fold over the level in dendritic cells (6.53 ± 1.12%) and 18.6-fold over that in T cells (1.47 ± 0.49%). The DiR^+ percentages in dendritic cells and T cells showed no significant difference from those in healthy controls. These results establish that systemically administered ELE-NE preferentially accumulates in intestinal macrophages during inflammation, underscoring its specific targeting toward inflammation-associated macrophages.

ELE-NE Ameliorates DSS-Induced Colitis in Mice

To assess the therapeutic efficacy of ELE-NE in colitis, we established a model by administering 2% DSS in the drinking water of C57BL/6J mice. Colitis mice received intravenous ELE-NE (5 mg/kg) every other day for a total of four doses, with age-matched healthy and untreated colitis mice serving as controls. All mice were analyzed on day 9 (Figure 5a). Given their central role in disease pathogenesis, we quantified colonic levels of key pro-inflammatory cytokines. ELE-NE treatment significantly suppressed IL-1β and IL-6 production, reducing them to approximately 26% and 22% of the levels in the untreated colitis group, respectively (Figure 5b). TNF-α levels were also markedly reduced, to about 32% of those in untreated controls (Figure 5c). These results confirm that ELE-NE alleviates intestinal inflammation by attenuating the production of pivotal pro-inflammatory cytokines.

https://doi.org/10.2147/IJN.S599389

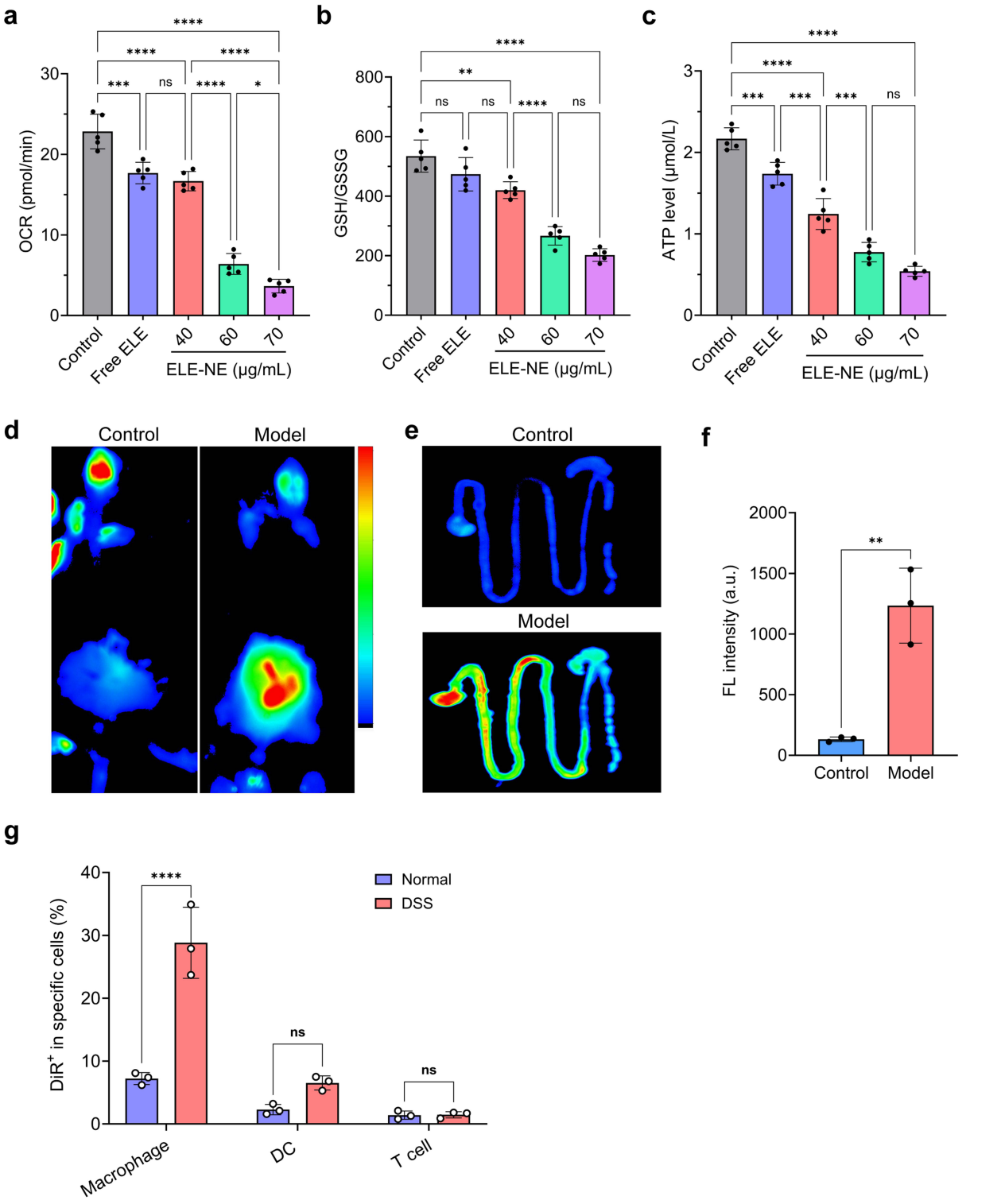

Figure 4 ELE-NE disrupts mitochondrial energetics in macrophages and exhibits targeted accumulation in inflamed colon. (**a**–**c**) LPS-induced M1 macrophages were treated with ELE-NE (40, 60, 70 μg/mL), β-elemene (70 μg/mL), or PBS. Shown are measurements of mitochondrial oxygen consumption rate (OCR) (**a**), GSH/GSSG ratio (**b**), and intracellular ATP levels (**c**) (n=5). (**d** and **e**) In vivo targeting of DiR-labeled ELE-NE (5 mg/kg, i.v.) in DSS-induced and healthy control mice. Near-infrared fluorescence images of the abdominal region (**d**) and isolated intestines (e) 24 h post-injection. (**f**) Quantification of intestinal fluorescence intensity (n=3). (**g**) Flow cytometric analysis of DiR^+ cells among intestinal immune cells from DSS-induced mice 24 h after DiR-ELE-NE injection (n=3). Data are representative of three biologically independent experiments. Data are shown as mean ± s.d., and statistical significance was determined by one-way ANOVA with Tukey's post hoc test (**a**–**c**) or unpaired two-tailed Student's *t*-test (**f** and **g**). Significance levels are indicated as *p < 0.05, **p < 0.01, ***p < 0.001, ****p < 0.0001, and ns (not significant).

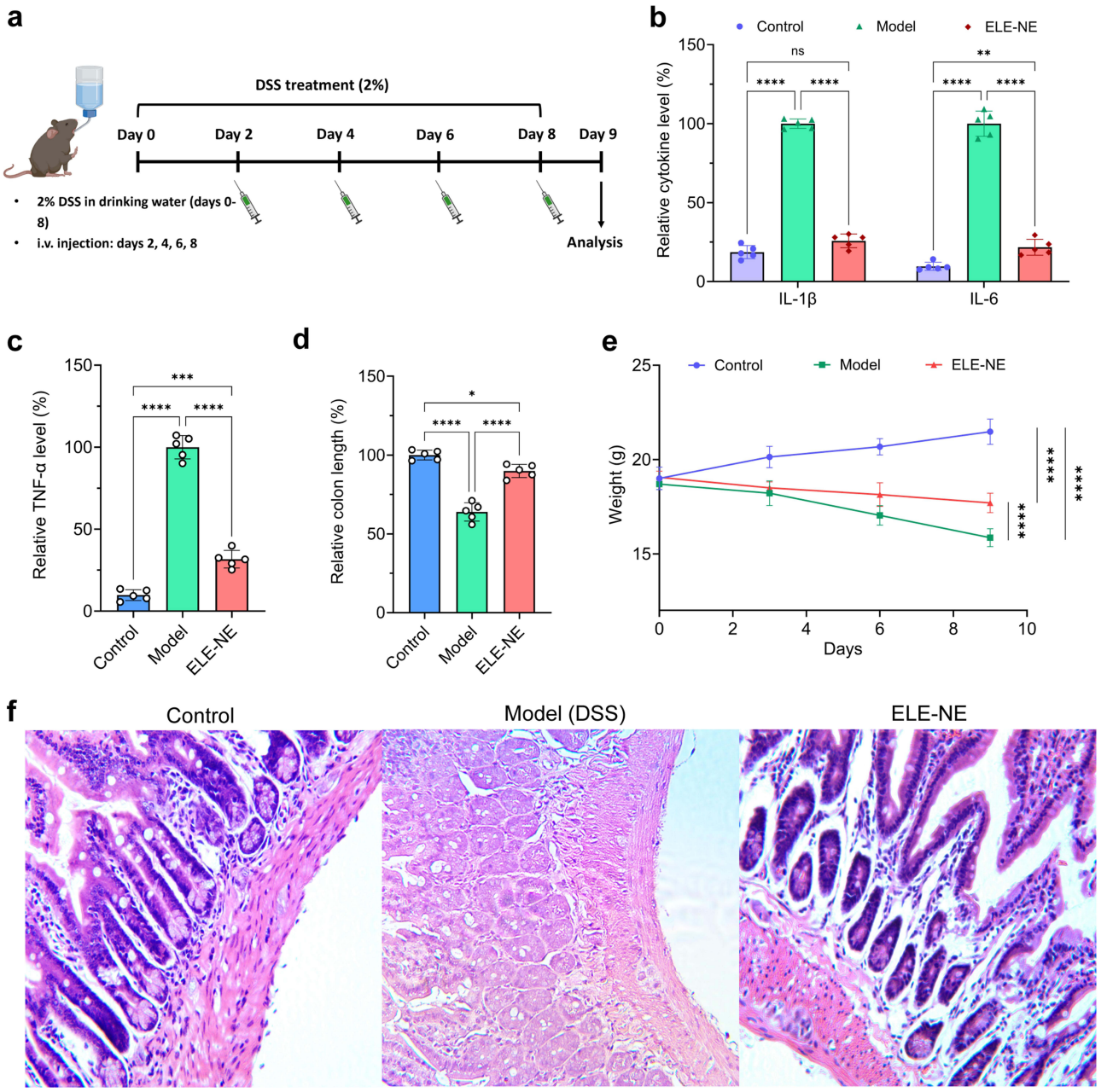

Figure 5 ELE-NE ameliorates ulcerative colitis in mice by suppressing colonic inflammation. (**a**) Mice received 2% DSS in drinking water for 8 days to induce colitis. From day 2, ELE-NE (5 mg/kg) or PBS was administered intravenously every other day (4 total doses). Each group contained at least five biologically independent mice. (**b** and **c**) ELISA quantification of pro-inflammatory cytokines in colon tissues: IL-1β and IL-6 (b), and TNF-α (c) (n=5). (**d**) Relative colon length in healthy, DSS, and ELE-NE-treated mice as a measure of tissue damage (n=5). (**e**) Body weight changes of healthy control mice, DSS-induced colitis model mice, and ELE-NE-treated colitis mice throughout the experimental period (n=5). (**f**) Representative H&E-stained colon sections from each group, showing tissue morphology and inflammatory infiltration. Data are representative of three independent experiments. Data are presented as mean ± s.d. Statistical analyses were performed using two-way ANOVA (**b** and **e**) and one-way ANOVA with Tukey's post hoc test (**c** and **d**). Significance levels are indicated as *p < 0.05, **p < 0.01, ***p < 0.001, ****p < 0.0001, and ns (not significant).

We next evaluated the therapeutic impact of ELE-NE by assessing key metrics of disease severity, including colon length, body weight, and histology. ELE-NE treatment markedly alleviated colon shortening, maintaining colon length at approximately 90% of healthy controls compared to 64% in DSS-treated mice (Figure 5d). ELE-NE treatment also mitigated body weight loss, sustaining a body weight of 17.7 ± 0.5 g in treated mice versus 15.9 ± 0.5 g in DSS controls by day 9 (approximately 93% of initial weight; Figure 5e).

Histological analysis of colon sections by H&E staining revealed severe inflammatory damage in DSS-treated mice, characterized by epithelial disruption and crypt distortion or loss (Figure 5f). ELE-NE treatment markedly attenuated

https://doi.org/10.2147/IJN.S599389

these pathological changes and promoted the restoration of epithelial and crypt architecture. Together, these findings demonstrate that ELE-NE effectively ameliorates DSS-induced colitis, as reflected by improved colon length, reduced weight loss, and preserved tissue integrity.

Safety Evaluation of ELE-NE

The clinical translation of systemically administered nanomedicines requires a thorough assessment of their in vivo biosafety. To evaluate the safety of ELE-NE, healthy C57BL/6J mice received intravenous injections of either PBS or ELE-NE (5 mg/kg). Serum was collected on day 9 for a comprehensive biochemical analysis. No significant differences were observed between the two groups across a panel of markers for hepatic injury (alanine aminotransferase, ALT; aspartate aminotransferase, AST), biliary function (total bilirubin, TB; direct bilirubin, DB), renal function (urea, creatinine), muscle damage (creatine kinase, CK), and general tissue stress (lactate dehydrogenase, LDH; total protein, TP) (Figure S2). These results confirm that a single course of ELE-NE treatment elicits no detectable hepatotoxicity, nephrotoxicity, or myotoxicity, supporting its favorable biosafety profile.

Discussion

β-Elemene, a sesquiterpene derived from Curcuma wenyujin, possesses diverse pharmacological activities.[39,66,67] However, its anti-inflammatory mechanism remains unclear, hindering clinical application. This study developed ROS-triggered ELE-NE and elucidated its mechanism of action in a colitis model. We uncover a novel therapeutic pathway where ELE-NE acts as a "mitochondrial metabolic disruptor" via ROS-triggered, aggregation-dependent mitochondrial targeting.

Mechanistically, ELE-NE exploits the pathological ROS burst in inflammatory macrophages. First, its designed microenvironment facilitates ROS-driven molecular aggregation of ELE, forming nanoscale aggregates (Figure 2b–d). Second, this aggregation is spatially confined to mitochondrial surfaces in M1 macrophages, as confirmed by colocalization and ROS-scavenging experiments (Figure 3a). Third, these aggregates directly disrupt the ETC, reducing OCR and ATP levels by approximately 84% and 75%, respectively, at a therapeutic concentration of 70 μg/mL (Figure 4a and c). Fourth, ETC dysfunction disrupts redox balance (reduced GSH/GSSG ratio, Figure 4b) and reprograms cellular metabolism, thereby abolishing M1 polarization. Consequently, ELE-NE potently suppresses pro-inflammatory cytokines (TNF-α, IL-1β, IL-6) to 16–20% of control levels in vitro and 22–32% in vivo (Figure 3c–e, 5b and c).

A key innovation is the identification of the olefinic (C=C) bond as a functional, bioresponsive motif. Unlike classic phytochemicals that bind signaling proteins,[68,69] the C=C moiety in ELE enables ROS-triggered self-aggregation, driving organelle-specific targeting. This insight extends to other olefin-rich natural products, suggesting a generalizable framework. We therefore propose the concept of "olefinic drugs"—a class of therapeutics that operate via mitochondrial metabolic reprogramming, complementing existing metabolic intervention strategies.

In vivo, ELE-NE showed targeted efficacy. It accumulated 9.4-fold higher in inflamed colon tissues than in healthy controls (Figure 4f), with specific targeting to intestinal macrophages (29% DiR^+ positive, Figure 4g). This precision translated to preserved colon length (~90% of healthy controls vs. 64% in the DSS group), reduced weight loss, and restored intestinal histology (Figure 5d–f), with no signs of systemic toxicity (Figure S2). In contrast to conventional biologics (eg., anti-TNF-α antibodies), which are associated with high costs, risk of immunogenicity, and primary or secondary loss of response, ELE-NE offers a distinct advantage through its low-cost potential, favorable safety profile, and a novel mechanism of metabolic reprogramming that addresses key limitations of current IBD therapies. Furthermore, we developed a ROS-activatable, mitochondria-targeted NIR fluorescent probe for non-invasive imaging, establishing a theranostic platform with clinical potential.

Looking forward, this work directly suggests two impactful research trajectories. First, applying the 'nano-confined aggregation' platform to other IBD-relevant immune cells (eg., T cells, dendritic cells, and M2 macrophages) will fully reveal its immunomodulatory scope. Second, and more broadly, the mechanistic principle we established provides a generalizable framework. In fact, other terpenes such as limonene and pinene have been reported to undergo radical polymerization or copolymerization via their C=C bonds under appropriate conditions, forming cross-linked networks—highlighting the intrinsic reactivity of the olefinic motif.[70] Extending this framework to diverse olefinic natural products promises to validate and ultimately expand the "olefinic drug" concept, potentially unlocking a new class of metabolism-targeted therapeutics.

Beyond these directions, further studies incorporating sex-specific validation, chronic colitis models, and head-to-head comparisons with standard therapies will be valuable to fully assess the translational potential of this platform.

In conclusion, we decipher a ROS-responsive mitochondrial targeting mechanism for β-elemene and establish the olefinic group as a novel bioresponsive pharmacophore. The proposed "olefinic drugs" concept establishes a new theranostic paradigm for treating inflammatory diseases through metabolic reprogramming.

Conclusion

In summary, this study elucidates a previously undefined anti-inflammatory mechanism of β-elemene. We demonstrate that its engineered nanoemulsion (ELE-NE) functions as a mitochondrial metabolic disruptor: it targets mitochondria in inflammatory macrophages and undergoes ROS-triggered, nano-confined aggregation at this site. This process impairs the electron transport chain, reprograms cellular energy metabolism, and alleviates experimental colitis. Complementing the therapy, a ROS-activatable, mitochondria-targeted NIR probe was developed, enabling non-invasive imaging and establishing a theranostic strategy. More broadly, our work redefines the olefinic (C=C) bond as a bioresponsive effector, thereby establishing the conceptual framework of "olefinic drugs." These findings advance the understanding of natural product immunomodulation and provide a generalizable blueprint for developing metabolism-targeted therapeutics.

Abbreviations

ALT, Alanine aminotransferase; ANOVA, One-way analysis of variance; AST, Aspartate aminotransferase; BSA, Bovine serum albumin; CREA, Creatinine; CK, Creatine Kinase; LDH, Lactate Dehydrogenase; TP, Total protein; CRE, Creatinine; TB, Total Bilirubin; DB, Direct Bilirubin; ELISA, Enzyme-linked immunosorbent assay; H&E, Hematoxylin and eosin; IFN-β, Interferon-β; IL-6, Interleukin-6; TEM, Transmission electron microscopy; TNF-α, Tumor necrosis factor-α; ELE-NE, elemene nanoemulsion; ROS, reactive oxygen species; ETC, electron transport chain; FBS, fetal bovine serum; M-CSF, macrophage colony-stimulating factor; LPS, lipopolysaccharide; APS, ammonium persulfate; TEMED, tetramethylethylenediamine; DLS, dynamic light scattering; GPC, Gel permeation chromatography; BMDM, mouse bone marrow-derived macrophages.

Data Sharing Statement

All data supporting the findings of this study are included within the manuscript and its supplementary information files. Additional data is available from the corresponding author Pengfei Zhang (zpf0418@i.smu.edu.cn) upon reasonable request.

Ethics Approval and Consent to Participate

All animal experimental procedures were approved by the Laboratory Animal Welfare and Ethics Committee of Southern Medical University (No. SMU20210851). All experiments complied with the Chinese Law on Laboratory Animal Welfare (Guideline for Ethical Review of Animal Welfare, Standard number: GB/T 35892-2018). The experimental mice were euthanized by cervical dislocation following anesthesia with isoflurane to minimize suffering.

Acknowledgments

We acknowledge the use of the Medpeer platform (https://www.medpeer.cn) for the creation of all schematic diagrams in this manuscript. All illustrations were originally generated through this platform and contain no third-party copyrighted material. This study was supported by the National Natural Science Foundation of China (32371518 and 32101209, P.Z.), the Science and Technology Program of Guangzhou (No.2025A04J5390, P.Z.) and the Guangdong Basic and Applied Basic Research Foundation (2023A1515012356, P.Z.).

Author Contributions

All authors made a significant contribution to the work reported, whether that is in the conception, study design, execution, acquisition of data, analysis and interpretation, or in all these areas; took part in drafting, revising or critically reviewing the article; gave final approval of the version to be published; have agreed on the journal to which the article has been submitted; and agree to be accountable for all aspects of the work. P.Z. and T.X. proposed the original concept of the study.

Funding

This study was supported by the National Natural Science Foundation of China (32371518 and 32101209, P.Z.), the Science and Technology Program of Guangzhou (No.2025A04J5390, P.Z.) and the Guangdong Basic and Applied Basic Research Foundation (2023A1515012356, P.Z.).

Disclosure

The authors report no conflicts of interest in this work.

References

1. Honap S, Jairath V, Danese S. et al. Navigating the complexities of drug development for inflammatory bowel disease. *Nat Rev Drug Discov*. 2024;23:546–562. doi:10.1038/s41573-024-00953-0
2. Wei Y, Fan Y, Ga Y, et al. Shaoyao decoction attenuates DSS-induced ulcerative colitis, macrophage and NLRP3 inflammasome activation through the MKP1/NF-κB pathway. *Phytomedicine*. 2021;92:153743. doi:10.1016/j.phymed.2021.153743
3. Khor B, Gardet A, Xavier RJ. Genetics and pathogenesis of inflammatory bowel disease. *Nature*. 2011;474:307–317. doi:10.1038/nature10209
4. Na YR, Stakenborg M, Seok SH, et al. Macrophages in intestinal inflammation and resolution: a potential therapeutic target in IBD. *Nat Rev Gastroenterol Hepatol*. 2019;16:531–543. doi:10.1038/s41575-019-0172-4
5. Le Berre C, Honap S, Peyrin-Biroulet L. Ulcerative colitis. *Lancet*. 2023;402:571–584. doi:10.1016/S0140-6736(23)00966-2
6. Abraham C, Cho Judy H. Inflammatory Bowel Disease. *N Engl J Med*. 2009;361:2066–2078. doi:10.1056/NEJMra0804647
7. Ardizzone S, Porro GB. Biologic Therapy for Inflammatory Bowel Disease. *Drugs*. 2005;65:2253–2286. doi:10.2165/00003495-200565160-00002
8. Deng F, He S, Cui S, et al. A Molecular Targeted Immunotherapeutic Strategy for Ulcerative Colitis via Dual-targeting Nanoparticles Delivering miR-146b to Intestinal Macrophages. *J Crohns Colitis*. 2019;13:482–494. doi:10.1093/ecco-jcc/jjy181
9. Mondal S, Das M, Ghosh R, et al. Chitosan functionalized Mn3O4 nanoparticles counteracts ulcerative colitis in mice through modulation of cellular redox state. *Commun Biol*. 2023;6:647. doi:10.1038/s42003-023-05023-6
10. Baumgart DC, Carding SR. Inflammatory bowel disease: cause and immunobiology. *Lancet*. 2007;369:1627–1640. doi:10.1016/S0140-6736(07)60750-8
11. Ji Y, Li X, Yao X, et al. Macrophage polarization: molecular mechanisms, disease implications, and targeted therapeutic strategies. *Front Immunol*. 2025;16:1732718. doi:10.3389/fimmu.2025.1732718
12. Yang K, Zhao Q, Sun Y, et al. Mitochondrial immunometabolism in sepsis: orchestrating macrophage polarization and dysfunction. *Eur J Med Res*. 2026;31:36. doi:10.1186/s40001-025-03590-4
13. Liu Y, Xu R, Gu H, et al. Metabolic reprogramming in macrophage responses. *Biomark Res*. 2021;9:1. doi:10.1186/s40364-020-00251-y
14. Casey AM, Ryan DG, Prag HA, et al. Pro-inflammatory macrophages produce mitochondria-derived superoxide by reverse electron transport at complex I that regulates IL-1β release during NLRP3 inflammasome activation. *Nat Metab*. 2025;7:493–507. doi:10.1038/s42255-025-01224-x
15. Thukral C, Cheifetz A, Peppercorn MA. Anti-Tumour Necrosis Factor Therapy for Ulcerative Colitis. *Drugs*. 2006;66:2059–2065. doi:10.2165/00003495-200666160-00002
16. Zhu S, Yang Z, Liu Y, et al. Oral Lipid Nanoparticles for Improving the Efficiency of Drug Delivery Systems in Ulcerative Colitis: recent Advances and Future Prospects. *Pharmaceutics*. 2025;17:547. doi:10.3390/pharmaceutics17050547
17. Huang Y, Wu Q, Li S, et al. Harnessing nature's pharmacy: investigating natural compounds as novel therapeutics for ulcerative colitis. *Front Pharmacol*. 2024;15:1394124. doi:10.3389/fphar.2024.1394124
18. Long D. Crohn's Disease and Ulcerative Colitis: from Pathophysiology to Novel Therapeutic Approaches. *Biomedicines*. 2024;12:689. doi:10.3390/biomedicines12030689
19. Kushwaha P, Qureshi R, Khan N, et al. Revolutionizing IBD therapy: insights into contemporary treatment strategies. *Int Rev Immunol*. 2026;45:1–25. doi:10.1080/08830185.2025.2563522
20. Fanizzi F, Peyrin-Biroulet L, Danese S, et al. Targeting the unmet needs in IBD: emerging therapies beyond biologics and small molecules. *Curr Opin Pharmacol*. 2025;85:102577. doi:10.1016/j.coph.2025.102577
21. Appiah JK, Hayat U, Garg N, et al. Emerging Therapies in Inflammatory Bowel Disease: a Comprehensive Review. *J Clin Med*. 2025;14:6119. doi:10.3390/jcm14176119
22. Liu C, Sun S, Feng Q, et al. Arsenene Nanodots with Selective Killing Effects and their Low-Dose Combination with ß-Elemene for Cancer Therapy. *Adv Mater*. 2021;33:2102054. doi:10.1002/adma.202102054
23. Rosillo MA, Sanchez-Hidalgo M, Cárdeno A, et al. Protective effect of ellagic acid, a natural polyphenolic compound, in a murine model of Crohn's disease. *Biochem Pharmacol*. 2011;82:737–745. doi:10.1016/j.bcp.2011.06.043
24. Kim G-Y, Kim K-H, Lee S-H, et al. Curcumin Inhibits Immunostimulatory Function of Dendritic Cells: mAPKs and Translocation of NF-κB as Potential Targets1. *J Immunol*. 2005;174:8116–8124. doi:10.4049/jimmunol.174.12.8116
25. Ji K, Gan X, Xu Y, et al. Protective effect of the essential oil of Zanthoxylum myriacanthum var. pubescens against dextran sulfate sodium-induced intestinal inflammation in mice. *Phytomedicine*. 2016;23:883–890. doi:10.1016/j.phymed.2016.05.006
26. Ninkuu V, Zhang L, Yan J, et al. Biochemistry of Terpenes and Recent Advances in Plant Protection. *Int J Mol Sci*. 2021;22:5710. doi:10.3390/ijms22115710
27. Tetali SD. Terpenes and isoprenoids: a wealth of compounds for global use. *Planta*. 2019;249:1–8. doi:10.1007/s00425-018-3056-x
28. Rivera Rodríguez R, Johnson JJ. Terpenes: modulating anti-inflammatory signaling in inflammatory bowel disease. *Pharmacol Ther*. 2023;248:108456. doi:10.1016/j.pharmthera.2023.108456
29. Luo L, Zhou J, Liu X, et al. Development of modern Chinese medicine guided by molecular compatibility theory. *J Adv Res*. 2025;73:713–728. doi:10.1016/j.jare.2024.08.005

30. Chen W, Li Y, Liu C, et al. In situ Engineering of Tumor-Associated Macrophages via a Nanodrug-Delivering-Drug (β-Elemene@Stanene) Strategy for Enhanced Cancer Chemo-Immunotherapy. *Angew Chem Int Ed*. 2023;62:e202308413. doi:10.1002/anie.202308413
31. Ji X, Tang Z, Liu H, et al. Nanoheterojunction-Mediated Thermoelectric Strategy for Cancer Surgical Adjuvant Treatment and β-Elemene Combination Therapy. *Adv Mater*. 2023;35:2207391. doi:10.1002/adma.202207391
32. Zhu Q, Yu C, Chen Y, et al. Dual mRNA nanoparticles strategy for enhanced pancreatic cancer treatment and β-elemene combination therapy. *Proc Natl Acad Sci*. 2025;122:e2418306122. doi:10.1073/pnas.2418306122
33. Chen J, Wang R, Wang T, et al. Antioxidant Properties of Novel Dimers Derived from Natural β-Elemene through Inhibiting H2O2-Induced Apoptosis. *ACS Med Chem Lett*. 2017;8:443–448. doi:10.1021/acsmedchemlett.7b00035
34. Liu M, Chen X, Ma J, et al. β-Elemene attenuates atherosclerosis in apolipoprotein E-deficient mice via restoring NO levels and alleviating oxidative stress. *Biomed Pharmacother*. 2017;95:1789–1798. doi:10.1016/j.biopha.2017.08.092
35. Sieniawska E, Michel P, Mroczek T, et al. Nigella damascena L. essential oil and its main constituents, damascenine and β-elemene modulate inflammatory response of human neutrophils ex vivo. *Food Chem Toxicol*. 2019;125:161–169. doi:10.1016/j.fct.2018.12.057
36. Liu J, Zhang Z, Gao J, et al. Downregulation effects of beta-elemene on the levels of plasma endotoxin, serum TNF-alpha, and hepatic CD14 expression in rats with liver fibrosis. *Front Med*. 2011;5:101–105. doi:10.1007/s11684-011-0111-4
37. Zhong Y, Liu J, Huo W, et al. β-Elemene reduces the progression of atherosclerosis in rabbits. *Chin J Nat Med*. 2015;13:415–420. doi:10.1016/S1875-5364(15)30034-0
38. Zhao Q, Chen L, Zhang X, et al. β-elemene promotes microglial M2-like polarization against ischemic stroke via AKT/mTOR signaling axis-mediated autophagy. *Chin Med*. 2024;19:86. doi:10.1186/s13020-024-00946-6
39. Fang Y, Kang Y, Zou H, et al. β-elemene attenuates macrophage activation and proinflammatory factor production via crosstalk with Wnt/β-catenin signaling pathway. *Fitoterapia*. 2018;124:92–102. doi:10.1016/j.fitote.2017.10.015
40. Liu L, Mao K, Wang W, et al. Kolliphor® HS 15 Micelles for the Delivery of Coenzyme Q10: preparation, Characterization, and Stability. *AAPS Pharm Sci Tech*. 2016;17:757–766. doi:10.1208/s12249-015-0399-5
41. Biasi F, Leonarduzzi G, Oteiza PI, et al. Inflammatory Bowel Disease: mechanisms, Redox Considerations, and Therapeutic Targets. *Antioxid Redox Signal*. 2013;19:1711–1747. doi:10.1089/ars.2012.4530
42. Jena G, Trivedi PP, Sandala B. Oxidative stress in ulcerative colitis: an old concept but a new concern. *Free Radic Res*. 2012;46:1339–1345. doi:10.3109/10715762.2012.717692
43. Campbell EL, Colgan SP. Control and dysregulation of redox signalling in the gastrointestinal tract. *Nat Rev Gastroenterol Hepatol*. 2019;16:106–120.
44. X-f Z, M-j D, Cheng C, et al. Andrographolide attenuates oxidative stress injury in cigarette smoke extract exposed macrophages through inhibiting SIRT1/ERK signaling. *Int Immunopharmacol*. 2020;81:106230. doi:10.1016/j.intimp.2020.106230
45. He T, Lin X, Su A, et al. Mitochondrial dysfunction-targeting therapeutics of natural products in Parkinson's disease. *Front Pharmacol*. 2023;14:1117337. doi:10.3389/fphar.2023.1117337
46. Han J, Wang J, Wang Y, et al. Sesquiterpene lactones-enriched fractions from Xanthium mongolicum Kitag alleviate RA by regulating M1 macrophage polarization via NF-κB and MAPK signaling pathway. *Front Pharmacol*. 2023;14:1104153. doi:10.3389/fphar.2023.1104153
47. Arshad L, Jantan I, Bukhari SNA, et al. Immunosuppressive Effects of Natural α,β-Unsaturated Carbonyl-Based Compounds, and Their Analogs and Derivatives, on Immune Cells: a Review. *Front Pharmacol*. 2017;8:22. doi:10.3389/fphar.2017.00022
48. Ge J, Liu Z, Zhong Z, et al. Natural terpenoids with anti-inflammatory activities: potential leads for anti-inflammatory drug discovery. *Bioorg Chem*. 2022;124:105817. doi:10.1016/j.bioorg.2022.105817
49. Wang Q, Wang Y, Liu S, et al. Theranostic nanoplatform to target macrophages enables the inhibition of atherosclerosis progression and fluorescence imaging of plaque in ApoE(−/−) mice. *J Nanobiotechnol*. 2021;19:222. doi:10.1186/s12951-021-00962-w
50. Chen W, Schilperoort M, Cao Y, et al. Macrophage-targeted nanomedicine for the diagnosis and treatment of atherosclerosis. *Nat Rev Cardiol*. 2022;19:228–249. doi:10.1038/s41569-021-00629-x
51. Hu C, Zhao X, Li J, et al. Preparation and characterization of β-elemene-loaded microemulsion. *Drug Dev Ind Pharm*. 2011;37:765–774. doi:10.3109/03639045.2010.541261
52. Lv B, Hou L, Zhang H, et al. Pimpinellin mitigates DSS-induced ulcerative colitis in mice by reducing inflammation and regulating gut microbiota. *Phytomedicine*. 2025;136:156308. doi:10.1016/j.phymed.2024.156308
53. Shirangi M, Sastre Toraño J, Sellergren B, et al. Methyleneation of Peptides by N,N,N,N-Tetramethylethylenediamine (TEMED) under Conditions Used for Free Radical Polymerization: a Mechanistic Study. *Bioconjugate Chem*. 2015;26:90–100. doi:10.1021/bc500445d
54. Peng X, Ren J, Zhong L, et al. Xylan-rich Hemicelluloses-graft-Acrylic Acid Ionic Hydrogels with Rapid Responses to pH, Salt, and Organic Solvents. *J Agric Food Chem*. 2011;59:8208–8215. doi:10.1021/jf201589y
55. Fujii S, Matsuzawa S, Nakamura Y. One-pot synthesis of conducting polymer-coated latex particles: ammonium persulfate as free radical initiator and chemical oxidant. *Chem Commun*. 2010;46:7217–7219. doi:10.1039/c0cc02005b
56. Stanford KR, Taylor-Clark TE. Mitochondrial modulation-induced activation of vagal sensory neuronal subsets by antimycin A, but not CCCP or rotenone, correlates with mitochondrial superoxide production. *PLoS One*. 2018;13:e0197106. doi:10.1371/journal.pone.0197106
57. Park W, Han Y, Kim S, et al. Antimycin A induces apoptosis in As4.1 juxtaglomerular cells. *Cancer Lett*. 2007;251:68–77. doi:10.1016/j.canlet.2006.11.002
58. Li J, Wang L, Wang B, et al. NOX4 is a potential therapeutic target in septic acute kidney injury by inhibiting mitochondrial dysfunction and inflammation. *Theranostics*. 2023;13:2863–2878. doi:10.7150/thno.81240
59. Kwesiga MP, Gillette AA, Razaviamri F, et al. Biodegradable magnesium materials regulate ROS-RNS balance in pro-inflammatory macrophage environment. *Bioact Mater*. 2023;23:261–273. doi:10.1016/j.bioactmat.2022.10.017
60. Chuang Y, Chang H, Li C, et al. Reactive Oxygen Species and Inflammatory Responses of Macrophages to Substrates with Physiological Stiffness. *ACS Appl Mater Interfaces*. 2020;12:48432–48441. doi:10.1021/acsami.0c16638
61. Sharma N, Akkoyunlu M, Rabin RL. Macrophages—common culprit in obesity and asthma. *Allergy Eur J Allergy Clin Immunol*. 2018;73:1196–1205. doi:10.1111/all.13369
62. Zorova LD, Popkov VA, Plotnikov EY, et al. Mitochondrial membrane potential. *Anal Biochem*. 2018;552:50–59. doi:10.1016/j.ab.2017.07.009

63. Varshney S, Kumar D, Choudhary R, et al. Flavopiridol inhibits adipogenesis and improves metabolic homeostasis by ameliorating adipose tissue inflammation in a diet-induced obesity model. *Biomed Pharmacother*. 2024;179:117330. doi:10.1016/j.biopha.2024.117330
64. Yan W, Li L, Ge L, et al. The cannabinoid receptor I (CB1) enhanced the osteogenic differentiation of BMSCs by rescue impaired mitochondrial metabolism function under inflammatory condition. *Stem Cell Res Ther*. 2022;13:22. doi:10.1186/s13287-022-02702-9
65. Wang S, Cai L, Ma Y, et al. Shaoyao decoction alleviates DSS-induced colitis by inhibiting IL-17a-mediated polarization of M1 macrophages. *J Ethnopharmacol*. 2025;337:118941. doi:10.1016/j.jep.2024.118941
66. Wu P, Cheng L, Liu Y, et al. Elemene mitigates oxidative stress and neuronal apoptosis induced by cerebral ischemia-reperfusion injury through the regulation of glutathione metabolism. *J Ethnopharmacol*. 2025;340:119166. doi:10.1016/j.jep.2024.119166
67. You J, Nguyen AV, Albers CG, et al. Wnt Pathway-Related Gene Expression in Inflammatory Bowel Disease. *Digest Dis Sci*. 2008;53:1013–1019. doi:10.1007/s10620-007-9973-3
68. O'Neill LAJ, Kishton RJ, Rathmell J. A guide to immunometabolism for immunologists. *Nat Rev Immunol*. 2016;16:553–565. doi:10.1038/nri.2016.70
69. Patra S, Muthuraman MS, Meenu M, et al. Anti-inflammatory effects of royal poinciana through inhibition of toll-like receptor 4 signaling pathway. *Int Immunopharmacol*. 2016;34:199–211. doi:10.1016/j.intimp.2016.02.027
70. Mosquera MEG, Jiménez G, Tabernero V, et al. Terpenes and Terpenoids: building Blocks to Produce Biopolymers. *Sustain Chem*. 2021;2:467–492. doi:10.3390/suschem2030026